An analysis of translation distance of tropical cyclones over the western North Pacific

Licheng Wang[1, 2], Xihui Gu[1, 3, 4*], Aminjon Gulakhmadov[5,6], Jianfeng Li[7], Louise J. Slater[4], Qiang Zhang[8, 9, 10*], Ming Luo[11], Guoyu Ren[1, 12], Dongdong Kong[1, 3], Yangcheng Lai[7], Jianyu Liu[12]

1. Department of Atmospheric Science, School of Environmental Studies, China University of Geosciences, Wuhan 430074, China;

2. CMA-NJU Joint Laboratory for Climate Prediction Studies, School of Atmospheric Sciences, Nanjing University, Nanjing 210023, China;

3. Centre for severe weather and climate and hydro-geological hazards, Wuhan 430074, China;

4. School of Geography and the Environment, University of Oxford, Oxford OX1 3QY, UK;

5. Research Center of Ecology and Environment in Central Asia, Xinjiang Institute of Ecology and Geography, Chinese Academy of Sciences, Urumqi 830011, China;

6. Institute of Water Problems, Hydropower and Ecology of the National Academy of Sciences of Tajikistan, Dushanbe 734042, Tajikistan;

7. Department of Geography, Hong Kong Baptist University, Hong Kong, China;

8. Key Laboratory of Environmental Change and Natural Disaster, Ministry of Education, Beijing Normal University, Beijing 100875, China;

9. Faculty of Geographical Science, Academy of Disaster Reduction and Emergency Management, Ministry of Education/Ministry of Civil Affairs, Beijing Normal University, Beijing 100875, China;

10. State Key Laboratory of Earth Surface Processes and Resources Ecology, Beijing Normal University, Beijing 100875, China;

11. School of Geography and Planning and Guangdong Key Laboratory for Urbanization and Geo-simulation, Sun Yat-Sen University, Guangzhou 510275, China;

12. Laboratory for Climate Studies, National Climate Center, China Meteorological

Administration, Beijing 100081, China;
13. Hubei Key Laboratory of Critical Zone Evolution, School of Geography and Information Engineering, China University of Geosciences, Wuhan, China.

*Corresponding authors:
E-mail addresses: guxh@cug.edu.cn (X. Gu) and zhangq68@bnu.edu.cn (Q. Zhang).

Abstract: Tropical-cyclone (TC) translation distance, proportional to its duration and translation speed, basically determines the spatial extent of TC impacted marine and terrestrial areas. Although a long-term slowdown of TCs has recently been reported, changes in translation distance of TCs over the western North Pacific (WNP) and their driving mechanisms remain poorly understood. Using multiple TC datasets, here we find that the trends are opposite in over-land translation distance of landfall WNP TCs over China and excluding China, with the number of landfalls in the two groups being almost the same. However, the increase in over-land translation distance of landfall TCs over China is offset by greater decrease in that excluding China, resulting in that over-land translation distance of TCs over the WNP has declined (-4.0% per decade). The over-sea translation distance of TCs over the WNP also shows a decreasing trend (-2.4% per decade), and thus the genesis-to-demise translation distance of TCs over the WNP has significantly decreased (by 17.7%) during 1961-2019. The shorter duration and reduced translation speed of TCs directly and jointly contribute (by 76.9% and 23.1%, respectively) to their shortened translation distance. The gradual increase in westerly and northerly winds and weaker moisture transport during the days following TC generation tend to inhibit long-distance travel after TC genesis. Declining TC translation distance is likely associated with the long-term increases in genesis potential index and an anomalous cyclonic steering flow over the WNP. Our findings suggest that these changes in TC translation distance may alter regional patterns of TC-related drying and wetting of the WNP.

Significance statement: The spatial extent affected by a tropical cyclone (TC) is largely determined by TC translation distance. For example, TCs passing through marine areas could cool sea surface temperature and modulate local air-sea heat fluxes exchange; TCs with longer translation distances over land are more likely to trigger widespread flooding or terminate droughts in inland areas. Over the western North Pacific (WNP), we find that observational evidence supports opposite trends in over-land translation distance of landfall TCs over China and excluding China. Nevertheless, the genesis-to-demise translation distance of TCs shows a significant decline over the WNP during the past six decades. Understanding the impacts of changes in TC translation distance has particular importance given the extensive footprint of TC-related drying and wetting of the marine and terrestrial areas.

Key words: Tropical cyclones; Translation distance; Attribution; Environmental changes; WNP

1. Introduction

Translation distance of tropical cyclones (TCs) largely determines their directly impacted marine and terrestrial areas. When a TC travels over the sea, it may cool local sea surface temperature and then modulate the air-sea heat fluxes exchange (Vincent et al. 2012; Sriver and Huber 2007; Schenkel and Hart 2015). Changes in TC translation distance may be related to the spatial patterns of TC tracks (Hiroyuki et al. 2020), which further affects the distribution of TC-induced drying and wetting (Enrico et al. 2020). For example, Enrico et al. (2020) found that TCs translating over the equatorial region of the west North Pacific (WNP) and inducing net eastward water translation anomalies in this region lead to drying the Maritime Continent atmosphere. On the other hand, TCs with longer over-sea translation distances have generally higher probability to be stronger when they make landfall, possibly due to that the oceans could supply more moisture and then enhance TC intensity (Li and Chakraborty 2020).

Heavy rainfall and subsequent flooding induced by TCs can cause widespread damages in both coastal and inland areas (Zhang et al. 2018, 2009; Czajkowski et al.

2013; Lai et al. 2020; Villarini et al. 2014). The spatial extents of TC-induced disasters are usually associated with TC translation distance, i.e. the longer the distance a TC travels, the larger the spatial extent it may affect in inland areas (Czajkowski et al. 2013; Villarini et al. 2014). For example, Typhoon Mangkhut (2018) developed in the WNP, traveled a long distance (i.e. 6933 km; above the 94th percentile of translation distance of all 954 WNP typhoons during 1961-2019), and triggered widespread major flooding in inland areas of China, such as Hunan province (Choy et al. 2020). Typhoon Cempaka (2021) formed in the South China Sea, moved slowly northwestward towards China, weakened rapidly after landfalling, and finally traveled a short distance (1585 km; below the 20th percentile) without producing serious damage.

The translation distance of a TC is determined by its duration and translation speed. Discussions about changes in TC duration and translation speed have received increasing attention. Studies have found that landfalling hurricanes from the North Atlantic decay more slowly over land in recent decades, and therefore last longer on land (Chavas and Chen 2020; Li and Chakraborty 2020; Zhu and Collins 2021). The climatic signature of this decay remains uncertain and unclear in other oceanic basins (Li and Chakraborty 2020). Observed global TC translation speed shows a slowdown of 10% over 1949-2016 that is the most pronounced (i.e. 21% reduction) for TCs over the WNP (Kossin 2018; Lai et al. 2020). However, the veracity of a global slowdown in TCs is still under debate, with discussions about the dependence of the decreasing trend on the choice of study period, as well as the uncertainty in TC track records caused by changes in TC monitoring technologies (e.g. satellite) over the past century (Chan 2019; Moon et al. 2019; Yamaguchi et al. 2020; Lanzante 2019). Changes in TC translation distance are the combined effect of changes in TC duration and translation speed, but given the uncertainties of changes in duration and translation speed, long-term changes in TC translation distance remain poorly understood. For example, Zhu and Collins (2021) found a significantly increased wind decay period of hurricanes over the continental United States during 1980-2019, which did not lead to changes in hurricane translation distance due to the impacts of translation speed. Chen et al. (2021) found that landfalling WNP TCs (tropical storms and typhoons) showed increased

intensity and duration over the mainland east and southeast Asia during 1979-2016, and hence increased TC impacts inland. Exploring the spatio-temporal characteristics of TC translation distance is therefore particularly important as it determines the areas that may be affected by TC impacts.

Using multiple TC best track datasets and ERA5 reanalysis data, we examine changes in TC translation distance over the past six decades and discuss possible physical mechanisms driving this change over the WNP, the region with the highest TC genesis in the world (i.e. about 1/3 of global TCs; Guo and Tan 2018). We provide observed evidence of changes in TC translation distance to improve scientific understanding of changes in TC-related risks and help elucidate the debate about long-term trends in TC motion with changes in environmental conditions.

2. Data

2.1 TC best track datasets

The WNP TC data are provided by four independent agencies, i.e. the China Meteorological Administration (CMA; Lu et al. 2021), the Regional Specialized Meteorological Center (RSMC) Tokyo-Typhoon Center of the Japan Meteorological Agency, the Joint typhoon Warning Center (JTWC), and the Hong Kong Observatory (HKO).

Table 1 shows the detailed information on these TC datasets. The maximum sustained wind speed that determines TC intensity (such as tropical depression, tropical storm, and typhoon) is averaged over a 10-minute period for the HKO and RSMC datasets, a 2-minute period for the CMA dataset, and 1-minute period for the JTWC dataset. The 10-minute period meets the demand of World Meteorological Organization and we therefore convert the maximum sustained wind speed in the CMA and JTWC datasets to the 10-mintue value by applying the conversion factors 0.96 and 0.93, respectively (Lee et al. 2012; Chen et al. 2021). It should be noted that the maximum sustained wind speed in the RSMC dataset is not available before the year 1977. The minimum sea level pressure is used to estimate the maximum sustained wind speed during the period 1961-1977 in the RSMC dataset, according to their relations proposed

by Atkinson and Holliday (1977).

Table 1 Information of the five TC datasets used in this study

Datasets	Record length	Temporal resolution	Maximum sustained wind speed	Conversion factor	Number of selected TCs	Source
CMA	1949-2020	6 hour	2 min	0.96	1586	China Meteorological Administration Tropical Cyclone Database
RSMC	1951-2020	6 hour	10 min	--	1524	Japan Meteorological Agency
JTWC	1945-2019	6 hour	1 min	0.93	1507	Joint typhoon Warning Center
HKO	1961-2019	6 hour	10 min	--	1434	Hong Kong Observatory
IBTrACS	1884-2019	3 hour	--	--	1414	National Oceanic and Atmospheric Administration

Note: The IBTrACS version 4 does not provide the maximum sustained wind speed values which are supplemented by the ensemble mean of maximum sustained wind speed from the CMA, RSMC, JTWC, and HKO datasets. The 3-hour IBTrACS TC dataset is not from observational records but interpolated based on the 6-hour records.

All four agencies provide TC best track positions and intensities for every six hours. The International Best Track Archive for Climate Stewardship (IBTrACS, Knapp et al., 2010) does not monitor TC position and intensity, but adjusts, compiles, and merges the available TC best tracks from the above four agencies to improve inter-agency comparisons. In the recently released version 4, IBTrACS only provides the merged TC positions without intensities (i.e. maximum sustained wind speed).

2.2 ERA5 reanalysis data

Hourly sea surface temperature (SST; units: K), sea level pressure (units: Pa), air temperature (units: K), meridional and zonal wind speed (units: m/s), convective available potential energy (units: J/kg), specific humidity (units: kg/kg), relative

humidity (units: %), vertical velocity (units: Pa/s), and vorticity (units: s^{-1}) data over 1961-2019 at 0.25°×0.25° spatial resolution are collected from the Medium-Range Weather Forecasts fifth generation atmospheric reanalysis dataset (ERA5, Hersbach et al., 2020). Note that the sea surface temperature is available at hourly resolution, but the content is only updated once daily.

2.3 ENSO and PDO indices

El Niño–Southern Oscillation (ENSO) is defined by the Niño 3.4 index. Monthly Niño 3.4 index and Pacific Decadal Oscillation (PDO) during 1961-2019 are obtained from Global Climate Observing System. El Niño and La Niña years and strength are determined using the Oceanic Niño Index (https://origin.cpc.ncep.noaa.gov/products/analysis_monitoring/ensostuff/ONI_v5.php).

3. Methods

3.1 Processing of TC best tracks

For the four best track TC datasets (i.e. CMA, RSMC, JTWC, and HKO), we first compile the tracks at regular six-hour intervals. Tropical depressions (i.e., TCs with maximum sustained wind speeds of less than 34 knots) are then removed from the TC datasets, because of large discrepancies in the numbers of tropical depressions among these datasets (Lee et al. 2012; Chen et al. 2021). Third, for each TC track in the four datasets, we exclude TC positions if they are recorded as an extratropical transition or if their maximum sustained wind speed is less than 20 knots (i.e. the lowest maximum sustained wind speed of a TC). The first and last positions of selected partial tracks (i.e., the TC tracks used in our analysis, hereafter) are labelled as the genesis and demise. After this processing, 1586, 1524, 1507, and 1434 TCs remain for our analysis in the CMA, RSMC, JTWC, and HKO datasets, respectively.

For the IBTrACS dataset, we select the same TCs which are recorded in the four other datasets. We then obtain 1414 TC best tracks in the IBTrACS dataset. These 1414 IBTrACS TCs do not include tropical depressions, as these were excluded in the

processing of the above four TC datasets. Similarly, TC positions that were recorded as an extratropical transition or where the maximum sustained wind speed was less than 20 knots in any of the four TC datasets are not included. This ensures the selected partial tracks in the IBTrACS dataset were confirmed by all four agencies, and also means that the TC translation distances in the IBTrACS dataset are shorter than those of the same TCs in all four other datasets. Taking Typhoon Khanun (2005) as an example, its selected partial track translation distance is 4159, 3088, 3342, and 3601 km in the CMA, RSMC, JTWC, and HKO datasets, but only 2426 km in the IBTrACS dataset which is 31.6% lower than the ensemble mean (i.e. 3547.5 km) of the four datasets (Table S1). Through these TC and partial track selection criteria, we minimize the impact of biases and heterogeneity in TC datasets on our results as much as possible.

3.2 Classification of TC paths and intensities

K-means clustering is a commonly used objective method to classify TC paths (Camargo and Sobel 2005; Nakamura et al. 2009; Elsner 2003). The approach takes the mean values of various samples as initial class centers. All samples are classified according to the distance between the sample and the class center, to reduce the classification error and then dynamically adjust the class center. The above steps are repeated to minimize classification error.

TC centroid position (i.e. longitude and latitude), length, direction, and curvature, are employed to classify TC paths. The centroid of one TC path is calculated by taking the maximum wind speed of TC centers as weights (Nakamura et al. 2009):

$$\vec{M}1 = \frac{1}{A}\int w(r)\vec{r}\,dxdy = \frac{1}{\sum_{i=1}^{n} w(r_i)}\sum_{i=1}^{n} w(r_i)\vec{r_i} \quad (1)$$

where $\vec{r}$ is the x and y coordinate vector on the path; $w(r)$ is the weight corresponding to each TC center; and, A is the standardized quantity reflecting total intensity of the TC. These TC paths are classified into three categories (west, west-north, and recurving paths) using the K-means clustering method, and the mean trajectory of these TC tracks in each category is estimated using the method proposed by Shen et al. (2018) (see Figs. S1 and S2).

3.3 Calculation of TC translation distance, duration and translation speed

A TC is identified as landfalling if any of its locations are over land (Kossin 2018). We used a high-resolution global topography map (2-Minute Gridded Global Relief Data; https://www.ngdc.noaa.gov/mgg/global/etopo2.html) to identify over-land TC positions (Fig. S3). Among the total 1414, 1586, 1524, 1507, and 1434 TCs from the IBTrACS, CMA, RSMC, JTWC, and HKO datasets, 879, 912, 899, 829, and 887 TCs were identified as landfalling TCs, respectively.

A TC track is split into segments using neighboring positions (i.e. each six-hour interval between two TC positions is a segment). For each segment of a TC, the distance between locations at both ends is calculated along a circle arc, and the translation speed is the distance divided by the time interval (i.e. six hours in this study). From a TC's genesis to its demise, we sum distances (durations) of all segments in the TC track as the TC translation distance (duration); similarly, we average translation speeds of all segments as the TC translation speed. Here, the translation distance, duration, and translation speed of all TCs are averaged in each year, respectively (Fig. 1a and c). We also analyze these TC motion characteristics for landfalling TCs (Fig. 1b and d), since (1) landfalling TCs were generally recorded with higher data quality than non-landfalling TCs; and (2) the longer translation distances of landfalling TCs usually have more widespread impacts on land, and especially inland areas.

For each TC segment, if either one or both of two positions are over land, then its translation distance, duration, and translation speed are considered as over-land values, or otherwise as over-sea values (Kossin 2018). We compute the translation distance, duration, and translation speed for each TC over land (the sea), and average them year-by-year, respectively. For TCs making more than one landfall or crossing small islands or archipelagoes, we employ the same approach to calculate over-land and over-sea values.

3.4 Change detection and statistical significance

Changes in the time series of annual-mean translation distance, duration, and

translation speed are detected using the modified Mann-Kendall method (Hamed and Rao 1998). The Pettitt method is used to detect abrupt change point in these time series (Pettitt 1979). This method is based on non-parametric detection of the mutation point of a time series, and provides the significance level (Pettitt 1979). The Student's *t* test is applied to investigate whether there is a significant difference between the mean values of two samples (Chand et al. 2017).

3.5 Relative contributions of TC duration and translation speed

Relative contributions of changes in TC duration and translation speed to changes in TC translation distance are estimated by using partial derivatives as suggested by Roderick et al. (2007). The annual average TC translation distance, duration, and translation speed are calculated as:

$$\begin{cases} D_i = \frac{\sum_j^{m_i} D_{ij}}{m_i} = \frac{\sum_j^{m_i} L_{ij} \times S_{ij}}{m_i} \\ L_i = \frac{\sum_j^{m_i} L_{ij}}{m_i} \\ S_i = \frac{\sum_j^{m_i} S_{ij}}{m_i} \end{cases} \quad (2)$$

where $D_i/L_i/S_i$ is the average TC translation distance/duration/translation speed of the *i*th year ($i = 1, \cdots, n$) and $D_{ij}/L_{ij}/S_{ij}$ is the translation distance/duration/translation speed of the *j*th TC ($j = 1, \cdots, m_i$) in the *i*th year. Given $D_i \approx L_i \times S_i = \widetilde{D}_i$ (see Fig. S4), we take the partial derivative with respect to time, *t*:

$$\frac{\delta \widetilde{D}}{\delta t} = \frac{\delta L}{\delta t}\bar{S} + \frac{\delta S}{\delta t}\bar{L} \quad (3)$$

where $\frac{\delta L}{\delta t}$ and $\frac{\delta S}{\delta t}$ are the slopes of annual average TC duration and translation speed, respectively; and $\bar{S}$ and $\bar{L}$ are their corresponding climatological means. Then, relative contributions of TC duration and translation speed to TC translation distance are estimated as:

$$\begin{cases} Con_L = \frac{\left|\frac{\delta L}{\delta t}\bar{S}\right|}{\left|\frac{\delta L}{\delta t}\bar{S}\right| + \left|\frac{\delta S}{\delta t}\bar{L}\right|} \\ Con_S = \frac{\left|\frac{\delta S}{\delta t}\bar{L}\right|}{\left|\frac{\delta L}{\delta t}\bar{S}\right| + \left|\frac{\delta S}{\delta t}\bar{L}\right|} \end{cases} \quad (4)$$

where Con_L and Con_S are the relative contributions of TC duration and translation

281 speed, respectively.

282

283 **3.6 Removal of the effect of climate modes**

284 The first-order effect of ENSO or PDO is reduced by developing the regression
285 between the annual index means during the TC season (July-October; Lee et al. 2010)
286 and the annual average TC translation distance, respectively (Wang and Toumi 2021;
287 Gudmundsson et al. 2017):

288 $$\widehat{D}_i = \beta_0 x_i + \beta_1 \quad (5)$$

289 where x is the time series of TC-season means of ENSO or PDO, respectively; and
290 β_0 and β_1 are the regression coefficients. The slope of the annual average TC
291 translation distance after removing ENSO and PDO effects is estimated from the time
292 series of $D_i - \widehat{D}_i$. Because of the epochal changes, the slope of the annual TC
293 translation distance in PDO neutral years (when TC-season means of PDO fall in the
294 range of -0.5℃ to +0.5℃) is also estimated (Wang and Toumi 2021).

295

296 **3.7 Large-scale environmental variables**

297 Steering flow is defined as mid-tropospheric (500 hPa) wind fields (Franklin et al.
298 1996; Chan and Gray 1982; Aryal et al. 2018). The steering flow is consistent with the
299 pressure-weighted deep-layer wind field between 300 hPa and 850 hPa (Aryal et al.
300 2018).

301 Vertical wind shear (units: m/s) is generally calculated using the wind field
302 between 200 hPa and 850 hPa (Zehr 2003):

303 $$v_{ws} = \sqrt{(u_{200} - u_{850})^2 + (v_{200} - v_{850})^2} \quad (6)$$

304 where u_{200} and u_{850} are the zonal wind (m/s) at 200 hPa and 850 hPa, respectively;
305 v_{200} and v_{850} are the meridional wind (m/s) at 200 hPa and 850 hPa, respectively.

306 The integrated vapor transport (IVT; units: $\mathrm{kg/(m \cdot s)}$) integrates specific
307 humidity, *U* wind, and *V* wind at multiple atmospheric levels from the surface to 300
308 hPa (Nayak et al. 2016):

309 $$IVT = \frac{1}{g}\int_{surface}^{300} \sqrt{(qu)^2 + (qv)^2}\ dp \quad (7)$$

where q, u, and v are specific humidity (kg/kg), and zonal and meridional wind (m/s), respectively; g is the gravity acceleration (m/s^2) and p is pressure.

The genesis potential index (GPI) is calculated based on a number of environmental variables and associated with TC generations (Emanuel 2007, 2005; Camargo et al. 2007a, 2007b):

$$GPI = |10^5\eta|^{3/2}\left(\frac{RH}{50}\right)^3\left(\frac{PI}{70}\right)^3(1+0.1v_{ws})^{-2} \quad (8)$$

where η is absolute 850-hPa vorticity (s^{-1}), and RH is 700-hPa relative humidity (%). PI (m/s) is the potential intensity (Emanuel 1995):

$$PI = \sqrt{\frac{T_S}{T_0}\frac{C_k}{C_D}[CAPE^* - CAPE]_m} \quad (9)$$

where T_S is sea surface temperature (K), T_0 is the outflow layer temperature (K), C_k is the exchange coefficient for enthalpy, C_D is the drag coefficient; $CAPE^*$ is the convective available potential energy (J/kg) of air saturated at sea surface temperature and lifted from sea level in reference to the environmental sounding, $CAPE$ is that of the boundary layer air (J/kg), and the subscript "m" indicates the values evaluated near the radius of maximum wind.

4 Results

4.1 Temporal changes in TC translation distance

Over the period 1961-2019 in the IBTrACS dataset, the translation distances of all and landfalling TCs over the WNP have significantly decreased by 17.7% (i.e. 3.0% per decade) and 33.6% (5.7% per decade), respectively (Fig. 1a and b). For the changes in the ensemble mean of TC translation distance from the four agencies (i.e. CMA, JTWC, RSMC, and HKO), significant decreasing trends are estimated as -1.8% and -2.2% per decade for all and landfall TCs, respectively (Fig. 1c and d). According to the Saffir–Simpson scale (Simpson and Riehl 1981), we select typhoons (1-min maximum sustained wind speed >64 kt) and detect changes in their translation distance (Fig. 2). Significant negative changes are also shown in typhoons from both IBTrACS and the ensemble mean of the four datasets. Specifically, the translation distances of typhoons and landfall typhoons decreased at rates of 2.3% and 2.7% per decade for the IBTrACS

dataset, respectively, as well as 1.9% and 2.0% per decade for the ensemble mean.

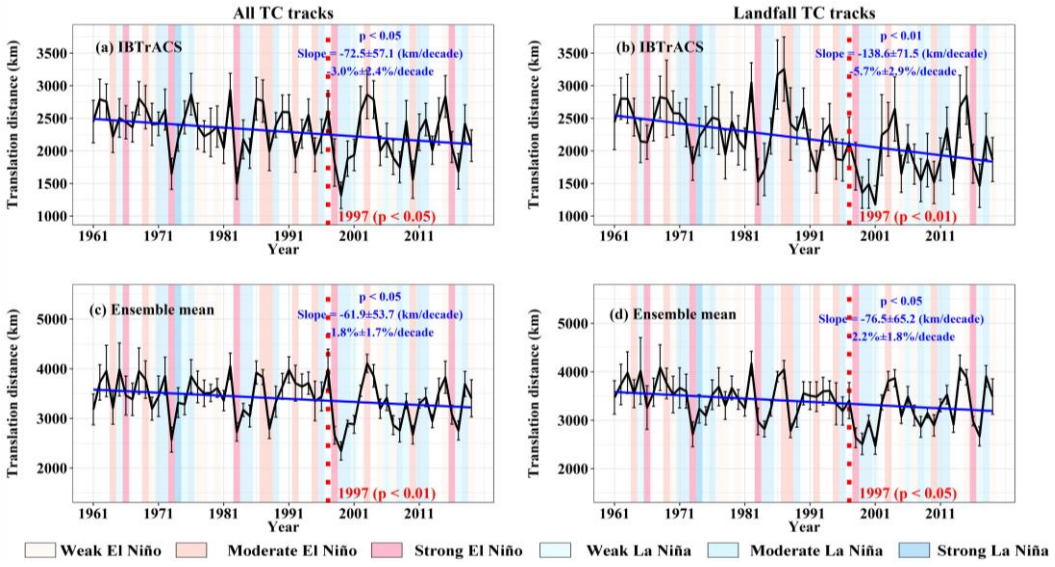

Fig. 1 Temporal changes in the annual-mean translation distance of tropical cyclones (TCs) over the western North Pacific (WNP) during 1961-2019: a and b are for all and landfalling TCs from the IBTrACS dataset; c and d are the same as a and b, but for ensemble mean of four TC datasets from CMA, JTWC, RSMC, and HKO, respectively (see Table 1 for details). Error bars indicate the 1 standard error of annual average translation distance. The vertical red dashed lines indicate whether there is an abrupt change point in the year 1997 in TC translation distance. Colored bars show the strengths of El Niño and La Niña events identified based on the Oceanic Niño Index (https://origin.cpc.ncep.noaa.gov/products/analysis_monitoring/ensostuff/ONI_v5.php).

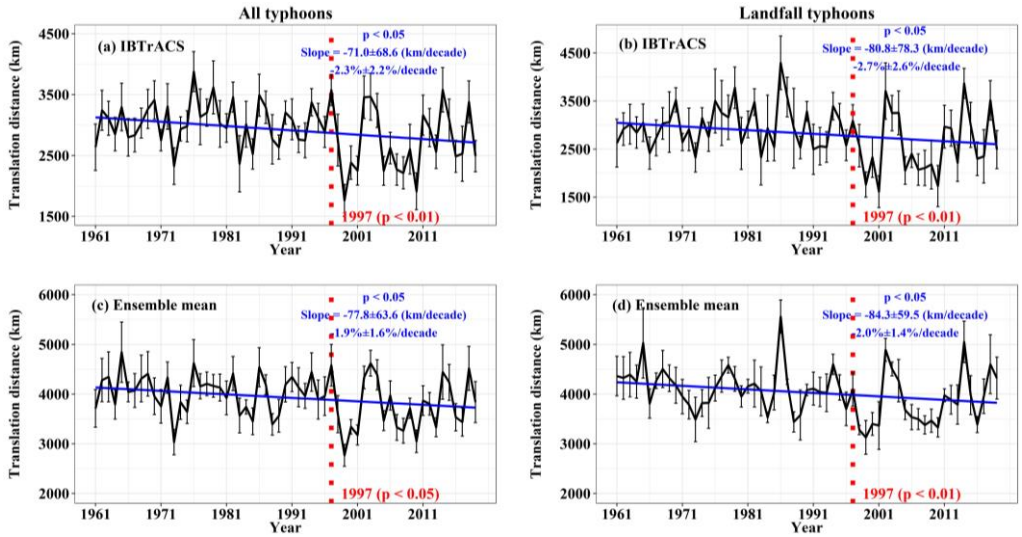

Fig. 2 The same as Fig. 1 but for typhoons.

We also detect whether the declining translation distance occurs in different categories of TC paths (Fig. 3). By using the K-means method, TC tracks over the WNP are classified into three categories: west path, moving straight westward to China and the Indochina peninsula; west-north path, moving northward and passing through

eastern China and the Korean peninsula; and recurving path, the tracks of TCs curved from northwest to northeast (Figs. S1 and S2). The mean trajectory of these TC tracks shows clear differences among the three categories. The results of our TC classification are consistent with those in previous studies despite using different clustering methods (Geng et al., 2017; Zhang et al., 2015). For example, Geng et al. (2017) classified the TC tracks that made landfall in China during 1951–2012 into three categories using a Finite Mixture Model algorithm, namely west (moving straightly westward), west-north (moving northwestward), and recurving paths (showing a parabolic-shape shift from northwest to northeast). Zhang et al. (2015) used fuzzy C-means to categorize TC tracks that made landfall in the Guangdong province in southeastern China into three categories: west path, north path, and recurving path.

We find the declining translation distance in all three categories of TC tracks as well as in both IBTrACS and multi-dataset ensemble mean (Fig. 3). Specifically, for the IBTrACS dataset, TC translation distance has significantly decreased at rates of 3.3%, 2.6%, and 2.9% per decade for west, west-north, and recurving paths, respectively. The values for the ensemble mean are 1.6%, 1.8%, and 2.7% per decade. Overall, our sensitivity analysis shows that these declining trends are systematically detected across different TC track datasets (except for HKO), paths, and intensities (Fig. 4a). Possible reasons for the opposite behavior in the HKO dataset are discussed below (see Discussion).

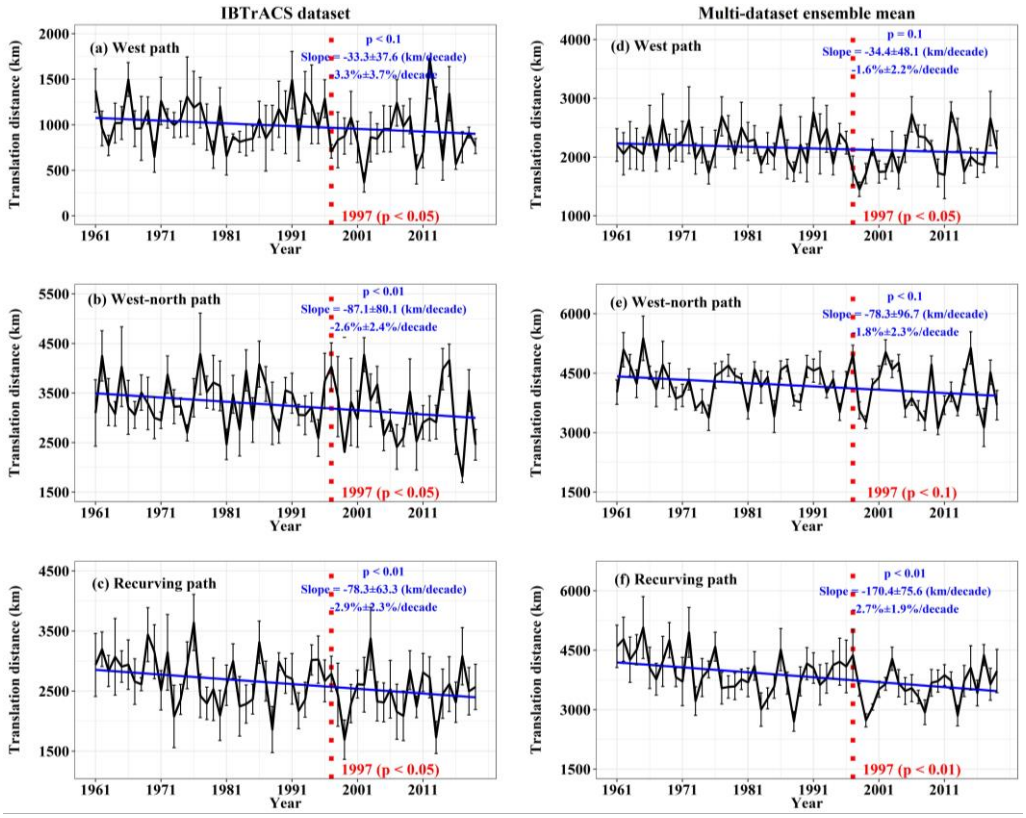

Fig. 3 The same as Fig. 1 but for west path, west-north path, and recurving path of TCs (see Figs. S1 and S2 for classification of the TC path categories), respectively.

Figs. 1-3 also clearly show inter-annual and inter-decadal variabilities in TC translation distance, which may be associated with ENSO and PDO (Lee et al. 2012). ENSO and PDO are two climate modes that modulate TC activity over the WNP (Wang et al. 2015; Wang and Liu 2016; Bell et al. 2014; Walsh et al. 2005; Camargo et al. 2007b). Evident interannual variability can be observed in WNP TC translation distance and anomalous decreases have been detected in years when strong El Niño events occurred, such as in 1997-1998 and 2015-2016 (Figs. 1 and 2). In El Niño phases, the WNP TC activities tend to be weakened due to large-scale circulation patterns, such as low-level divergence, weaker convective activity, and less energy and vapor moisture over the WNP (Zhang et al. 2018; Corporal-Lodangco et al. 2016).

Over the period 1961-2019, the PDO shifted from a warm to a cold phase in the late 1990s coinciding with abrupt changes in WNP TC activities. This consistency between the shifted regime in the PDO and TC activities (such as translation speed, coastward migration, and frequency of occurrence) in the 1990s has been recently

documented (He et al. 2015; Lanzante 2019; Wang and Toumi 2021). For example, He et al. (2015) detected an evident decrease of TC genesis number over the WNP after the year 1997; Wang and Toumi (2021) also found a migration of TCs toward coasts during 1999-2018 relative to 1982-1999. These studies revealed that the changes in TC activity and behind TC-related atmospheric circulation anomalies were related to the phase shift of the PDO. Consistently, we also detect a significant abrupt change in the year 1997 in TC translation distance using the Pettitt method (Figs. 1-3). Therefore, we split the whole dataset into two sub-periods, i.e. pre- and post-change point periods (1961-1997 and 1998-2019). In comparison with the pre-change point period, the mean translation distance of all (landfalling) TCs is significantly shorter in the post-change point period across different TC track datasets (except for HKO), paths, and intensities (Fig. 4d). For example, the annual-mean translation distance of all TCs in the IBTrACS dataset (multi-dataset ensemble mean) significantly decreased from 2369 (3494) km to 2168 (3222) km and by 8.4% (7.7%). The relations between ENSO and PDO and TC translation distance as well as physical mechanisms should be further investigated, but are beyond the scope of our study.

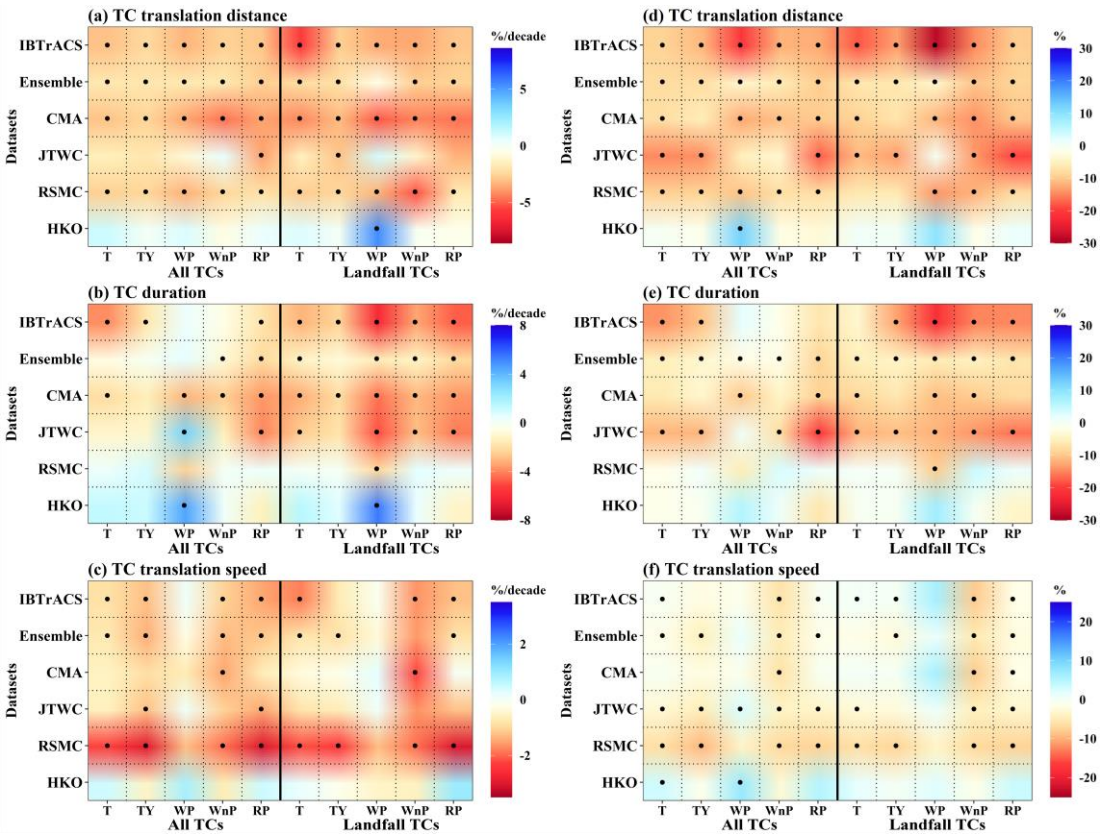

Fig. 4 Changes in TC translation distance, duration, and translation speed over the WNP during 1961-2019. a-c are the long-term trends (units: %/decade) and d-f are the relative changes (units: %) between 1961-1997 (before the change point) and 1998-2019 (after the change point). The black dots indicate the changes at the 95% confidence level. T, TY, WP, WnP, and RP indicate total TCs, typhoons, west paths, west-north paths, and recurving paths, respectively. "Ensemble" indicates the multi-dataset ensemble mean.

4.2 Attribution of changes in TC translation distance to TC duration and translation speed

Both IBTrACS and the multi-dataset ensemble mean show that all and landfalling TCs have become shorter-lasting (Fig. 5a-d) and slower-moving (Fig. 5e-h; also see Lai et al. 2020; Kossin 2018). The decreases in TC duration and translation speed can be observed across different TC track datasets (except for HKO), paths, and intensities (Fig. 4b and c). Similar to TC translation distance, inter-annual and inter-decadal variabilities occur in both TC duration and translation speed. For example, an abrupt change point in the year 1997 is also detected in TC duration and translation speed. From the pre- to post-change point periods (1961-1997 to 1998-2019), both TC duration and translation speed are dominated by decreases (Fig. 4e and f). Therefore, the decreases in TC duration and translation speed, as the principal controlling factors of translation distance, explain the reduction of TC path lengths.

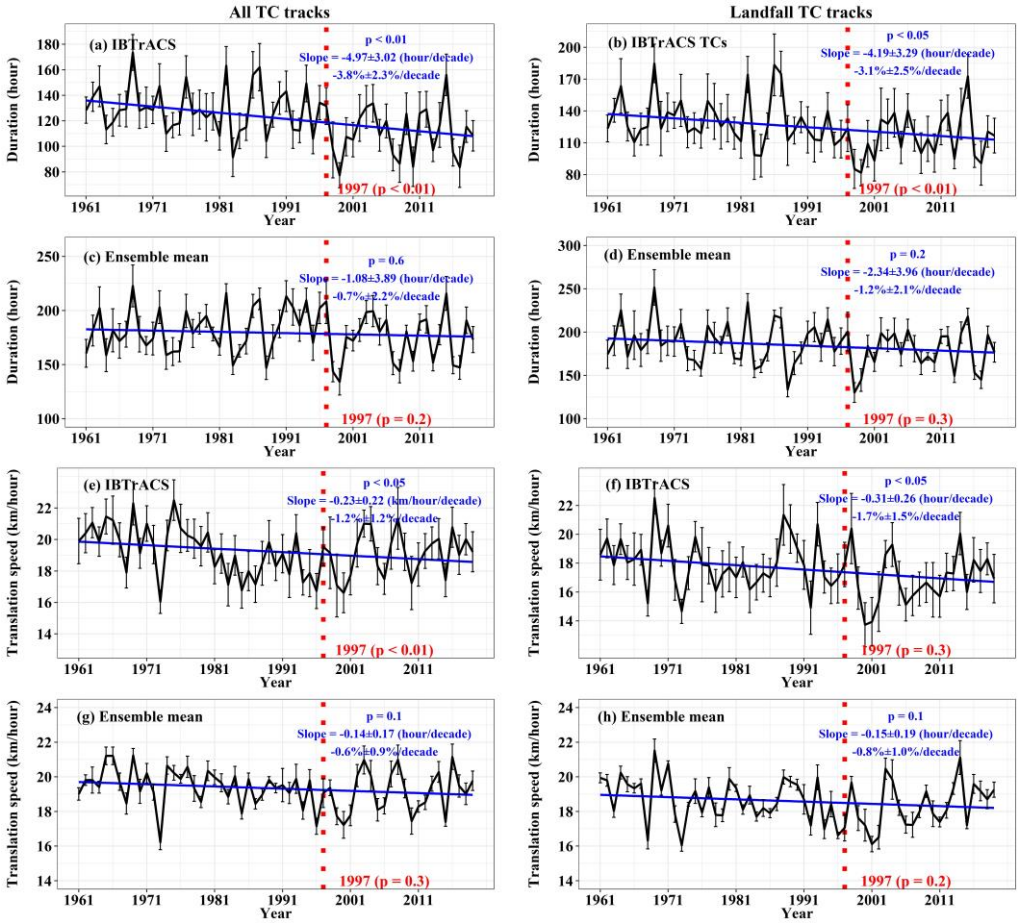

Fig. 5 The same as Fig. 1 but for TC duration (a-d) and translation speed (e-h).

The WNP region (including terrestrial and oceanic areas) is divided into 10°×10° grids. We count the translation distance, duration, and translation speed of each TC track within each 10°×10° grid (see Fig. S5 with Typhoon Khanun as an example). Then, we calculate annual average values of translation distance, duration, and translation speed for each grid, respectively. The 10°×10° grid cell size is a compromise between reducing spatial variability (smaller grids generally lead to larger variability in TC motion features) and the desire to obtain more grids over the WNP. Through binning locations of TC circulation centers into 10°×10° grids, we further analyze the spatial pattern of changes in TC translation distance, duration, and translation speed (Fig. 6 and Fig. S6). The trend in annual average TC translation distance is detected grid by grid. There is an obvious spatial heterogeneity of the changes in TC translation distance (Fig. 6a). The terrestrial areas prone to TCs (especially southeastern Asia) are

dominated by decreasing TC translation distance. In contrast, the oceanic areas display an uneven change pattern, with decreasing TC translation distance mainly in the western WNP, the region with the most WNP TC geneses (Corporal-Lodangco et al. 2016). Overall, the declining rate of TC translation distance over land is -4.0% per decade ($p < 0.05$), which is almost twice that over the sea (-2.4% per decade, $p < 0.05$) (Fig. 6d), suggesting a faster shortening of translation distance after TCs have made landfall.

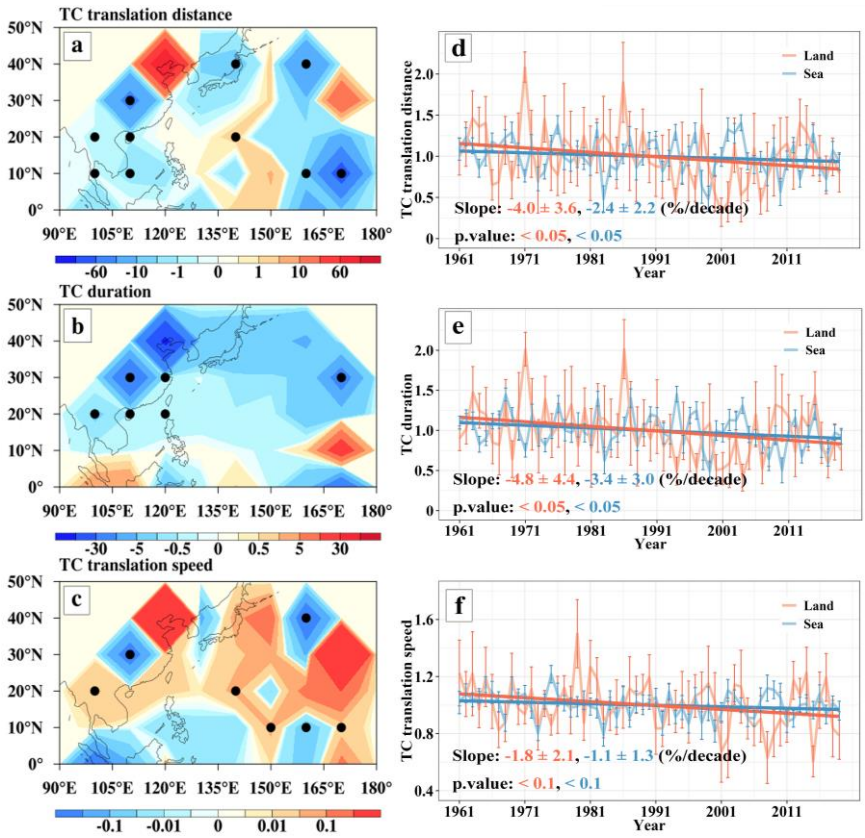

Fig. 6 Spatio-temporal changes in TC translation distance (km per decade), duration (hours per decade), and translation speed (km/hour per decade) of WNP TCs during 1961-2019 from the IBTrACS dataset. In a, b, and c, the locations of TC centers are binned into 10°×10° grids; annual-mean TC translation distance, duration and translation speed are calculated in each grid, and their trends are detected grid by grid. The stippling in a, b, and c indicates that the trends are significant at the 90% confidence level. For d, e, and f, the annual-mean TC translation distance, duration and translation speed are averaged and then normalized over the land and sea for the entire region separately; error bars indicate 1 standard error of the annual-mean values.

In line with the TC translation distance, faster significant decreases in TC duration and translation speed are found over land (-4.8% per decade and -1.8% per decade,

respectively) than over the sea (-3.4% per decade and -1.1% per decade, respectively) (Fig. 6e and f). The recent changes indicate that over-land TC segments now tend to linger longer, last less time, and then move with a shorter distance than the segments over the sea. The Spearman's correlation between the spatial patterns of TC translation distance and TC duration is 0.87 (Fig. 6a and b), which is much higher than that between TC translation distance and TC translation speed (i.e. 0.68; Fig. 6a and c), implying that the decrease in TC duration plays a more important role in the shortening of TC translation distance. We quantify the contributions of TC duration and translation speed to the declining TC translation distance using partial derivatives (see Methods; Table 2). Based on the IBTrACS dataset/multi-dataset ensemble mean, the relative contributions of the decreases in TC duration and translation speed to the shortening of the TC translation distance are 76.9%/65.3% and 23.1%/34.7%, respectively.

Table 2 Relative contributions of the changes in TC duration and translation speed to the declining TC translation distance during 1961–2019

Category	Duration	Translation speed
All TCs	76.9%/65.3%	23.1%/34.7%
Landfall TCs	67.7/60.3%	32.3%/39.7%
TY	89.0%/81.1%	11.0%/18.9%
Landfall TY	77.2%/50.5%	22.8%/49.5%
West path	25.6%/56.3%	74.4%/43.7%
West-north path	56.2%/32.3%	43.8%/67.7%
Recurving path	88.5%/82.3%	11.5%/17.7%

Note: "xx/xx" indicates the results based on the IBTrACS/multi-dataset ensemble mean.

Chen et al. (2011) reported increased over-land duration of TCs that made landfall over mainland China during 1975-2009 based on the CMA dataset. We repeat the approach in Chen et al. (2011) based on all five datasets (Fig. S7). An increased over-land duration of landfall TCs over China during 1961-2019 and 1975-2009 is found in the CMA, RSMC, and IBTrACS datasets, while a decreased trend is found in the JTWC and HKO datasets (see the left column of Fig. S7). If we exclude tropical depressions in these TCs, all datasets (except HKO) show increased over-land duration of landfall TCs over China during 1975-2009 (see the middle column of Fig. S7). However, if we count the over-land duration of TCs (excluding tropical depressions) over the WNP, all

the datasets (except RSMC) show decreased trends during 1975-2009 (see the right column of Fig. S7). This decreasing trend also occurs in all five datasets during 1961-2019. These results confirm decreased over-land duration of TCs over the WNP during 1961-2019. The difference in TC numbers over China and the WNP is an important reason for the opposite trends in over-land TC duration between our results and Chen et al. (2011). After excluding tropical depressions during 1961-2019, landfall TCs over China are 451, 474, 470, 439, and 440 in the CMA, RSMC, JTWC, HKO, and IBTrACS datasets, accounting for 49.5%, 52.7%, 56.7%, 49.5%, and 50.1% of all WNP landfall TCs in the five datasets, respectively. In other words, nearly half of TCs (i.e. excluding landfalling TCs over China) contribute to the decreased over-land duration.

Chen et al. (2021) reported an increase in over-land translation distance of TCs over the mainland of east and southeast Asia during 1979-2016, mainly due to the increase in over-land duration of TCs. This result does not seem to agree with ours, because the criteria for selecting TCs differ. Specifically, Chen et al. (2021) excluded TCs that made landfall more than once or only crossed islands or archipelagoes; and, they only considered the over-land translation distance for TC positions with intensity exceeding 17 m/s. These criteria make the number of their selected TCs notably smaller than ours (see Fig. 2A in Chen et al. (2021) and Fig. S1 in our study), and their over-land TC duration (around 10 hours; Fig. 4B in Chen et al. (2021)) also substantially lower than ours (around 20 hours in Fig. S7). These distinct differences lead to the discrepancy in changes of over-land TC translation distance.

As mentioned before, there are opposite trend directions of duration between landfall TCs over China and excluding China, as well as translation distance. We therefore split landfall TCs into two groups: passing through China mainland (group 1; the left column in Fig. S8) and non-passing through China mainland (group 2; the right column in Fig. S8). The numbers of landfall TCs in the two groups are almost 1:1. It can be seen from Fig. S8 that TC paths in group 1 are dominated by west-north tracks while the group 2 consists of west (mainly passing through southeastern Asia) and recurving (mainly passing through Japan and Korean Peninsula) paths. We further analyze changes in TC motion between the two groups (Figs. S9-S12).

Indeed, opposite trend directions occur in over-land translation distance between landfall TCs over China and excluding China, as well as duration and translation speed (Figs. S9 and S10). Specifically, significantly increased over-land duration of landfall TCs over China is found in both IBTrACS (2.5% per decade, $p < 0.05$) and ensemble mean of the four datasets (3.6% per decade, $p < 0.01$), while the two change rates for that excluding China are -2.6% per decade ($p < 0.05$) and -3.3% per decade ($p < 0.01$), respectively (Fig. S9c and d). The above changes in over-land TC duration are consistent with those in the four track datasets (Fig. S10e-h). Over-land translation distance of landfall TCs over China shows non-significant increase in the ensemble mean (1.9% per decade, $p = 0.3$) but non-significant decrease in IBTrACS (-0.8% per decade, $p = 0.7$) (Fig. S9a). Among the four track datasets, only CMA show significant increase (3.5% per decade, $p < 0.05$) in over-land translation distance of landfall TCs over China, JTWC and HKO show non-significant increase (i.e. 1.8% and 1.7% per decade, respectively; both $p = 0.4$), and RSMC shows non-significant decrease (i.e. -0.2% per decade, $p = 0.9$) (Fig. S10a-d). However, both ensemble mean and IBTrACS show significant decrease in over-land translation distance of landfall TCs excluding China (i.e. -3.2% and -3.1% per decade, respectively; Fig. S9b), which is confirmed by all the four track datasets (Fig. S10a-d). The slight increase in over-land translation distance of landfall TCs over China is offset by greater decrease in that excluding China (Fig. S9a and b), and thus the over-land translation distance over the WNP shows decreased trend (Fig. 6d).

When focusing on the whole translation distance, duration, and translation speed (i.e. from the genesis to the demise; see Section 3.1) of landfall TCs over China and excluding China (Figs. S11 and S12), decreased translation distance and duration are found in landfall TCs both over China and excluding China. These decreases occur in IBTrACS, ensemble mean, and almost all the four datasets (Figs. S11 and S12). This indicates that translation distance and duration of landfall TCs over the WNP show decreased trends during 1961-2019 no matter they pass through China or not. This result enhances the robustness of our finding on the declining translation distance of TCs over the WNP.

4.3 Dynamics behind the decline of TC translation distance

The declining TC translation distance is partly due to the northwestward shift of mean generation location (Fig. 7a and b and Fig. S13). We observe a significantly decreasing trend in the average generation longitude of TCs, and significantly increasing trend in the generation latitude, suggesting that there has been a migration of the WNP TCs toward the coasts. Additionally, both the original and detrended TC translation distances significantly positively (negatively) relate to the TC generation longitude (latitude) (Tables S2 and S3). The northwestward generation of TCs leads to a decrease in the distance of TC genesis location to land, as a consequence of shortening TC translation distance over the sea (Fig. 6d). Moon et al. (2019) compared the global over-sea TC position points between the pre-satellite era (1949-1965) and the post-satellite era (1982-2016) and found significant increases in the total number of over-sea positions with the increasing availability of satellite images. This indicates that more over-sea (especially pelagic) TC positions have been missed in the pre-satellite era, implying that the locations of TC genesis could have greater longitude and lower latitude than the recorded values. In other words, the northwestward trend of TC genesis during the 1961-2019 may be underestimated.

With the exception of west-path TCs, we also find positive correlations between TC translation distance and TC termination locations for west-north and recurving paths (Tables S2 and S3). The termination locations of west and west-north paths have moved northwestward (Fig. 7c-f); however, the resistance effect of the elevated terrain on the western part of East Asia limits the movement of TCs into inland areas (Chen and Wu 2016). The recurving TCs terminate southwestward (Fig. 7g and h), along with northwestward genesis locations (Fig. 7a and b), explaining their shortening translation distance (Fig. 3c).

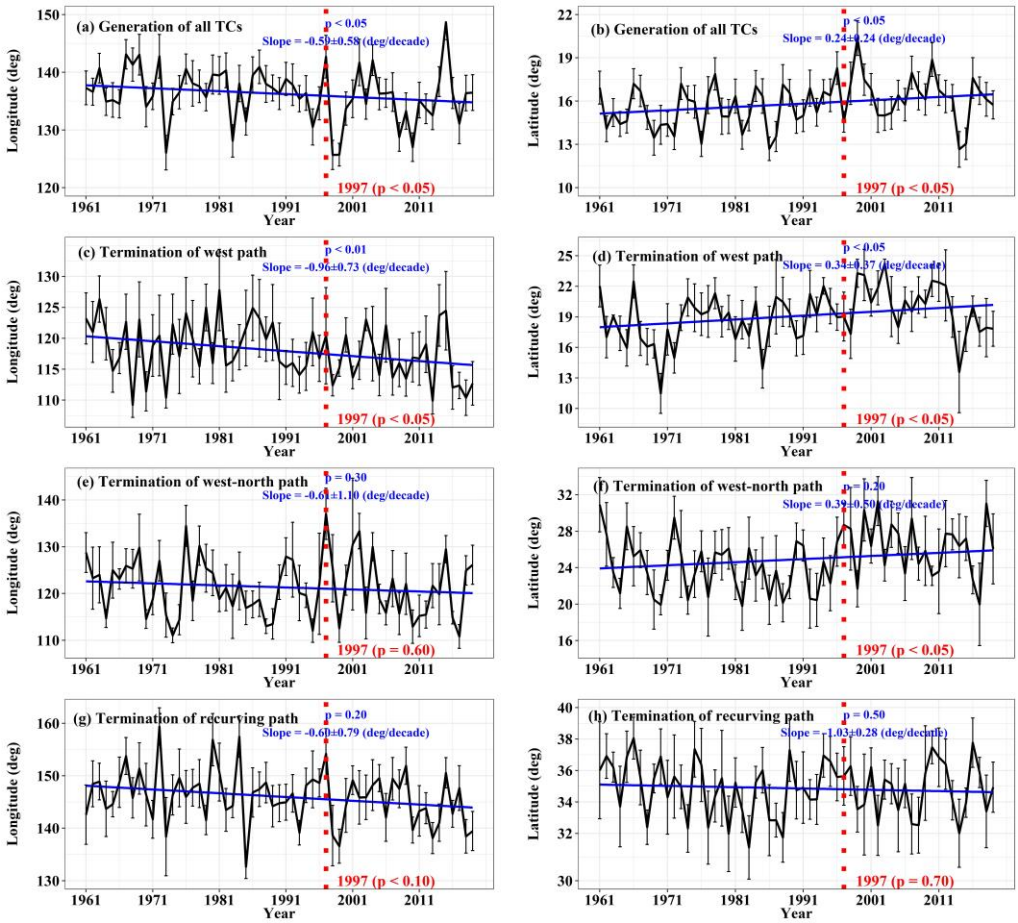

Fig. 7 Temporal changes in location (i.e. longitude and latitude) of TC generations and terminations over the WNP during 1961-2019 from the IBTrACS dataset. Error bars indicate 1 standard error of annual average longitude/latitude.

Since TC motion is primarily determined by the steering flow and water vapor transport guiding their tracks and defining their thermal structure and intensity in the middle and lower troposphere (Wang and Wu 2004; Emanuel et al. 2004, 2008; Wang and Toumi 2021), we first examine daily composite evolutions of these factors after TC generation (Fig. 8). After TC generation, the westerly winds progressively strengthen against the westward movement of TCs (Fig. 8a-c). The areas with westerly winds expand as TCs development, and move northward as TC positions northward. Meanwhile, we also observe strengthening northerly winds over the 90°-130°E, the dominant region which 67% of total TCs pass through. The strengthening westerly and northerly winds push against the direction of TC movements, likely hindering their movement to the coast and inland areas. On the other hand, the integrated vapor

transport weakens gradually over 15-45°N (especially over the East Asia land areas) after TC generation (Fig. 8d-f). This weakening moisture transport over land and offshore areas does not contribute to providing energy supply or maintaining TC intensity. The evolution of steering flow and integrated vapor transport after generation tends to inhibit a long-distance TC travel.

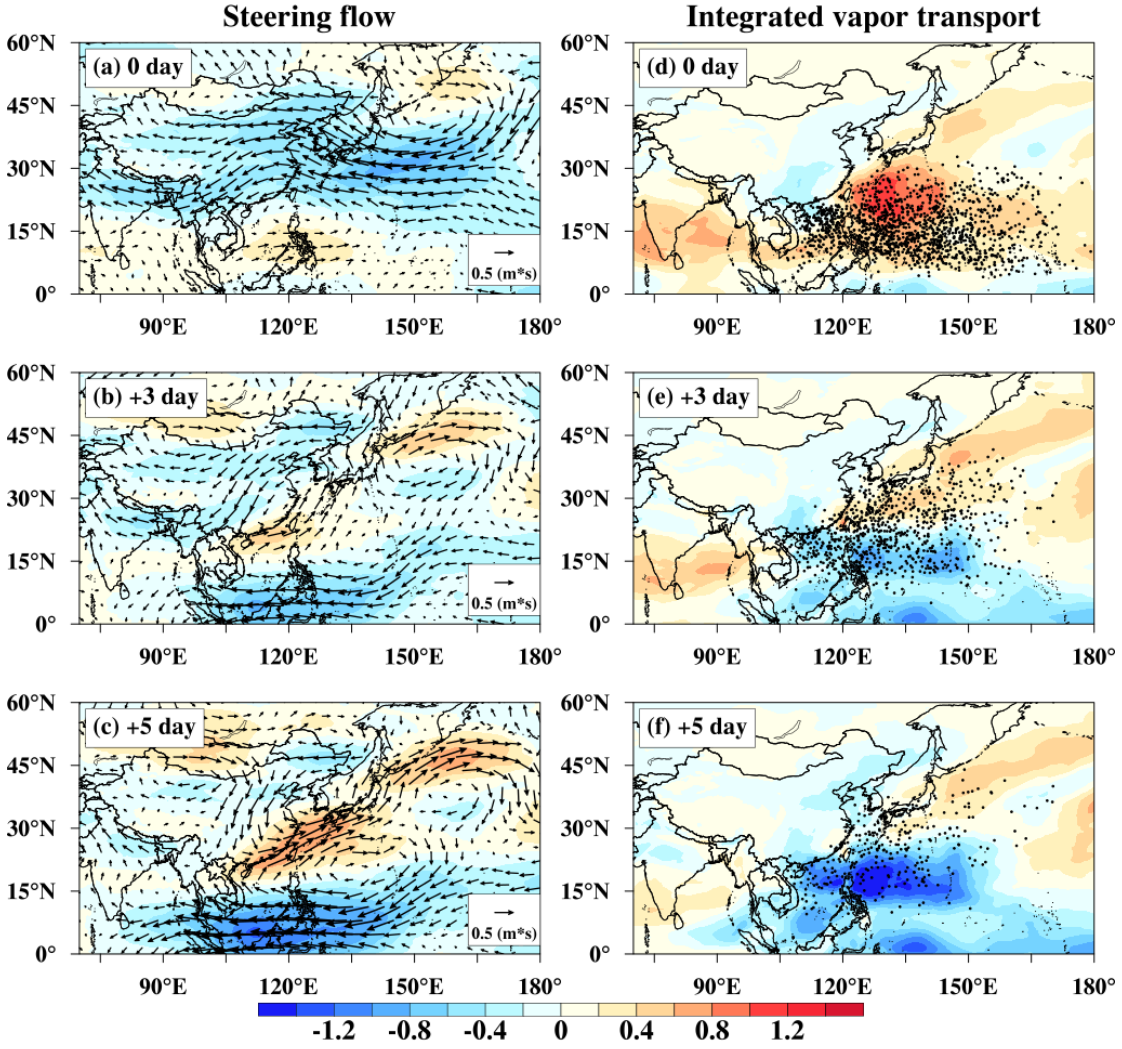

Fig. 8 Composite evolution of steering flow (arrows, units: m/s; colored shadow, zonal steering flow) and integrated vapor transport (IVT; units: 100 kg/(m · s)) anomalies after the generation of IBTrACS TCs over the WNP during 1961-2019. Daily data for the period 1961-2019 are employed for the composite analysis. 0 day indicates the day of TC generation, and +3 and +5 days are the post-*n* days of TC generation, respectively. Composite values are calculated by averaging the variable on all 0, +3, and +5 days in the period of analysis, respectively. Composite anomalies are differences between composite values and the average of all 0 days during the reference period 1961-1990. In d-f, the black dots are the TC locations in the corresponding day.

In addition to the evolution of steering flow and integrated vapor transport within

a 5-day window, we also assess the declining climatology of TC translation distance by exploring the relative changes between pre- and post-change point periods (1961-1997 and 1998-2019) and the long-term trends of key large-scale environment variables, including GPI, relative humidity, zonal and meridional wind of steering flow, and vertical wind shear during 1961-2019 (Fig. 9 and Fig. S14). These variables have been shown to closely relate to TC intensity and motion (Frank and Ritchie 2001; Chan and Gray 1982; Franklin et al. 1996; Zehr 2003). Relative to the pre-change point period, GPI values significantly increase in the post-change point period over western WNP adjacent to southeastern China (i.e. 15°-30°N; Fig. 8a), indicating increases of TC geneses over this region and thus decreases of distance to land (Fig. 7a and b). Steering flow over the western WNP becomes significantly eastward and southward (see the anomalous cyclonic anomaly), opposing the westward and northward translation of TCs, which is likely to further obstruct TC motion in the later period (Fig. 9d). Relative humidity significantly decreased in the post-change point period over the land areas of East Asia (Fig. 9b). The lower the relative humidity in the middle troposphere, the weaker the TC intensity (Chan and Gray 1982; Emanuel et al. 2004). The decrease in relative humidity also means less water vapor supply for TCs, which is unconducive to TC development, subsistence, and hence translation. For southeastern Asia and the areas which the recurving TCs mainly pass through (e.g. Japan), the vertical wind shear is enhanced during the second period compared to the first period (Fig. 9c). This enhanced vertical wind shear is not beneficial to maintain the warm-core structure of TCs (Cheung 2004; Frank and Ritchie 2001; Zehr 2003). These large-scale circulation patterns drive a rapid departure of latent heat from the disturbance area in the troposphere due to condensation, such that heat can no longer be concentrated in the middle and upper troposphere.

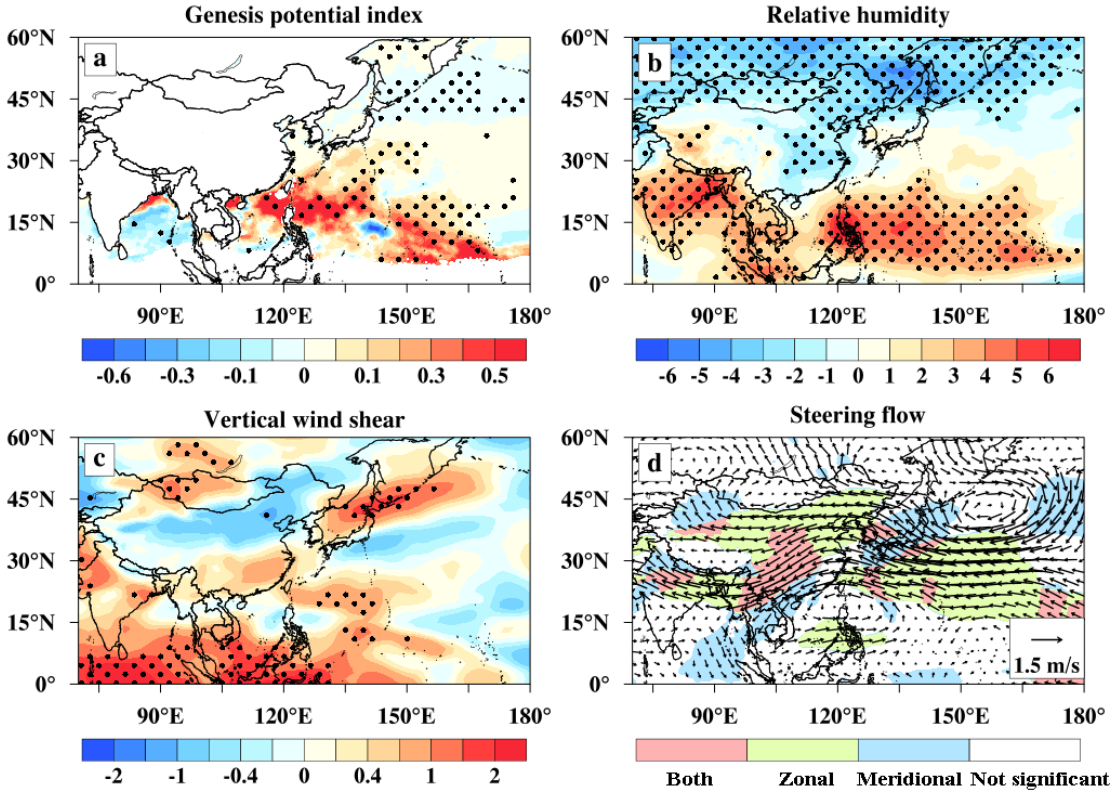

Fig. 9 Relative changes in genesis potential index (a), relative humidity (b, %), vertical wind shear (c, m/s), and steering flow (d; zonal and meridional components, arrows, m/s) between pre- and post-change point periods (i.e. 1961-1997 and 1998-2019). Values are calculated by averaging the variable on all days of TC lifetime in each year, and relative changes are the differences in the values between pre- and post-change point periods. The stippling indicates the relative changes are significant at the 90% confidence level. In d, the colored shadow indicates the significance of difference in zonal (meridional) steering flow: "Both" indicates the significant in both zonal and meridional steering flow, "Zonal"/"Meridional" indicates the significant in only zonal/ meridional steering flow, and "Not significant" indicates the significant in neither zonal nor meridional steering flow.

The long-term trends of these large-scale environmental variables during 1961-2019 (Fig. S14) show consistent spatial patterns with those shown in Fig. 9. Over the last six decades, relative humidity has significantly increased in the Pacific warm pool with warming SSTs, enhancing abundant water vapor in the lower layer (Fig. S14b). This increasing water vapor is more likely to accumulate unstable energy, the release of which enhances precipitation anomalies, resulting in the release of latent heat of condensation, and forming a heat source in the troposphere. This heat source forces the airflow to form a strong low-level WNP cyclone anomaly over the western WNP (see steering flow in Fig. 9d and Fig. S14d), which is directly induced by moisture

accumulation through a Mastsuno-Gill type response and local air-sea interaction.

We use the Linear Baroclinic Model (LBM) to demonstrate the linear atmospheric response to diabatic heating (Watanabe & Jin, 2003). Forced by idealized diabatic heating centered at 0.45 sigma, the LBM is run for 30 days, and the atmospheric response at the 25th day is shown in Fig. S15, as the LBM model has already reached a steady solution after about 15 days of integration (Sun et al. 2010). Wind vectors in the middle troposphere (i.e. 500 hPa) display an obvious cyclonic anomaly northwest of the diabatic heating as a Rossby wave response, which confirms the low-level WNP cyclone anomaly of steering flow over western WNP (Fig. 9d). This cyclonic circulation forced by the diabatic heating is associated with increasing water vapor and release of unstable energy, and corresponds with decreases in TC translation speed and distance.

We finally discuss possible reasons for the regional variation of landfall TC translation distance. Previous studies have a consensus that the TC locations including both genesis and lifetime maximum intensity tend to be poleward migrations (Wang and Toumi 2021; Liu and Wang 2020; Kossin et al. 2014; Studholme et al. 2022). Wang and Toumi (2021) found that the distance between lifetime maximum intensity of global TCs and land has been shortened by about 30 km per decade during 1982-2018. Our results show that the genesis of TCs over the WNP are significantly northwestward (Fig. 7a and b). Liu and Wang (2020) found significantly increased landfall latitude and intensity of TCs over China during 1980-2017. The poleward migration of TC locations over the WNP tends to reduce the translation distance at low latitudes (e.g. southeastern Asia) on one hand, and to enhance the translation distance at middle latitudes (e.g. northern China) on the other hand. Studholme et al. (2022) pointed out that the poleward expansion of TC latitudes would lead to more mid-latitude areas experiencing TCs, which is consistent with the increased TC translation distance in northern China (Fig. 6a).

Changes in large-scale environmental variables can also partly explain the regional variation of landfall TC translation distance. For example, the abnormal cyclonic steering flow over the southeastern Asia (Fig. 9d) hampers TCs to more westward and

684 then is beneficial for the reduction in translation distance of landfall TCs over
685 southeastern Asia (Fig. 6a). We also notice that the change pattern of vertical wind shear
686 is basically consistent with that of TC translation distance (Fig. 6a and Fig. 9c).
687 Specifically, vertical wind shear shows decrease in northern China and increase in
688 southwestern WNP and in northwestern WNP (e.g. Korean Peninsula and Japan);
689 observed increased (decreased) TC translation distance occurs in northern China
690 (southwestern and northwestern WNP). Reduced (enhanced) vertical wind shear is (not)
691 favorable for TC development (Wang and Toumi, 2021). More specific reasons for the
692 regional variation of landfall TC translation distance over the WNP should be explored
693 by using model simulations in the future.
694
695 **5. Discussion**
696 The inhomogeneity in TC track data is generally known to affect estimated trends
697 in TC motion (Chan 2019; Moon et al. 2019). This inhomogeneity includes track
698 observation differences among different datasets (see Fig. S16 for year-to-year number
699 of all and landfall TCs in the five datasets) and TC monitoring technology upgrades
700 over past decades. Impacts of inhomogeneity in TC tracks on changes in TC motion
701 have been intensely disputed, especially regarding the veracity of a global slowdown in
702 TC translation speed (Kossin 2018; Chan 2019; Moon et al. 2019; Lanzante 2019).
703 Some decreasing TC motion, especially TC translation speed, is likely tied to natural
704 internal climate variability, such as ENSO and PDO (Lanzante 2019). The sensitivity
705 of our results to data inhomogeneity and natural internal climate variability is discussed
706 herein.
707
708 **5.1 Uncertainties in TC track observations**
709 TC monitoring entered the post-satellite era after the introduction of satellite
710 remote sensing in 1965 and measurements with global coverage became available from
711 1981 (Lanzante 2019; Moon et al. 2019). Only the HKO dataset shows a nonsignificant
712 increasing TC translation distance during the period 1961-2019, due to the abnormally
713 low values during 1961-1980 in comparison with the other datasets (Fig. S17). The bias

714 in TC tracks mainly occurs in the pre-satellite era, due to the dramatic increase in the
715 annual number of over-sea positions (Moon et al. 2019). We count the annual
716 percentage of WNP TC position points over the sea to total points in the five datasets
717 (Fig. S18). The most dramatic fluctuation in the annual percentage of over-sea points
718 to total points is found in the HKO dataset, indicating larger systematic biases existing
719 in the TC tracks between pre- and post-satellite eras. We also test changes in TC
720 translation distance during the period 1981-2019, and find consistent decreases in TC
721 translation distance (Figs. S19), demonstrating that the downward trend in TC
722 translation distance over the WNP is robust. We notice that the HKO dataset shows
723 decreases in translation distance of all and landfall TCs and typhoons in the post-
724 satellite era (i.e. 1981-2019).
725
726 **5.2 Impacts of climate modes**
727 Since ENSO and PDO are the dominant natural variabilities affecting TC activities
728 as discussed above, we remove their first-order effects in the trend evaluation. We find
729 that significant downward trends are still detected after the first-order effects of ENSO
730 and PDO are removed (Table 3). Considering PDO epochal changes, we also evaluate
731 the changes in TC translation distance in PDO neutral years and note that the trends are
732 still downward. These results suggest that the downward trend in WNP TC translation
733 distance cannot be fully explained by natural internal climate variability.
734 We evaluate the association between shortening TC translation distance and the
735 changes in circulation patterns, such as steering flow and vertical wind shear. The TC
736 circulation changes have also previously been qualitatively linked with natural
737 variabilities, such as the PDO (Yang et al. 2018; Wang et al. 2015). Other studies have
738 tried to attribute changes in TC motion (such as translation speed) to anthropogenic
739 warming by using numerical simulations of Global Climate Models (GCMs) (Zhang et
740 al. 2020; Lai et al. 2020; Yamaguchi et al. 2020). However, because the number of high-
741 resolution GCMs available for TC simulations and tracking is still limited (Knutson et
742 al. 2020, 2019), the attribution of changes in TC motion to anthropogenic warming is
743 not robust and even contradictory in previous studies (Knutson et al. 2013; Yamaguchi

et al. 2020; Zhang et al. 2020). For example, by using the same GCM (Meteorological Research Institute–Atmospheric General Circulation Model version 3.2), Zhang et al. (2020) found a slowdown of TC motion under future anthropogenic warming (Zhang et al. 2020), while Yamaguchi et al. (2020) reported translation speed was expected to increase (Yamaguchi et al. 2020). Therefore, the reasons for the changes in circulation patterns related to TC motion and the role of anthropogenic warming require further exploration in future studies.

Table 3: Trends (km/decade) in the translation distance of WNP TCs during 1961-2019 before and after removing the impacts of ENSO and PDO separately

Dataset	Category	All TCs	Landfall TCs	Typhoons	Landfall Typhoons	West path	West-north path	Recurving path
IBTrACS	Original	-72.5*	-138.6**	-71.0*	-80.8*	-33.3	-87.1**	-78.3**
	ENSO-removed	-80.4**	-135.2**	-80.1**	-93.4**	-92.3**	-96.5**	-80.3**
	PDO-removed	-77.6**	-138.6**	-77.5*	-105.9**	-25.2	-69.1	-81.1**
	PDO neutral years	-191.5*	-265.7**	-43.6	20.8	-133.1**	-70.9	-188.9
Ensemble mean	Original	-61.9*	-76.5*	-77.8*	-84.3*	-34.4	-78.3	-170.4**
	ENSO-removed	-78.6**	-90.7**	-95.3**	-122.2**	-39.8	-92.9**	-135.1**
	PDO-removed	-79.2*	-87.1**	-91.3**	-116.9**	-36.5	-83.2*	-119.5**
	PDO neutral years	-187.7	-212.2	-132.0	-202.9	-179.2	-223.6	-352.8**

Note: **/* indicates the trend in TC translation distance is significant at the 0.01/0.05 level.

6. Conclusions

In this study, we analyzed translation distance of TCs over the WNP based on multiple TC track datasets from the IBTrACS and four independent agencies. We find that over-land translation distance of landfall TCs over China shows an increasing trend during 1961-2019 while it is opposite to that of landfall TCs excluding China. The numbers of landfall TCs over China and excluding China are almost the same; however, the increase in over-land translation distance of landfall TCs over China is offset by greater decrease in that excluding China, as a consequence of declining over-land translation distance of TCs over the WNP. We discuss that this regional variation of landfall TC translation distance may be associated with poleward migration of TC

locations over the WNP. The poleward migration of TCs tends to limit (enhance) their translations at low (middle) latitudes.

Nevertheless, both the IBTrACS dataset and multi-dataset ensemble mean show a significant decrease in translation distance of TCs over the WNP during 1961-2019. Spatially, TC translation distance over land has declined (-4.0% per decade) almost two times faster than over the sea (-2.4% per decade). The decreases in TC duration and translation speed directly lead to the shortening of translation distance, and TC duration plays a dominant role. The gradual increase in westerly and northerly winds and weaker moisture transport during the days following TC generation tend to inhibit long-distance travel after TC genesis. From the viewpoint of long-term changes in large-scale environmental variables, the western WNP show increases in genesis potential index and an anomalous cyclonic steering flow, and the land areas of East Asia show decreases in relative humidity and increases in vertical wind shear, collectively driving the declining TC translation distance over the WNP.

Our work reveals that observational evidence supports a significant decline in the translation distance of WNP TCs during the last six decades (1961-2019). It should be noted that this decline is spatially uneven for over-land translation distance. In general, TCs with longer over-land translation distance are more likely to travel deep inland and cause flooding over large inland areas (Villarini et al. 2014; Czajkowski et al. 2013); for example, Typhoon Nina from the WNP in 1975 moved into central China, resulting in catastrophic flooding and 26,000 fatalities (Yang et al. 2017). Conversely, TCs moving a long distance over land can also terminate inland droughts (Kam et al. 2013; Maxwell et al. 2013), as highlighted by the negative relations between TC frequency and mid-latitude drought in East Asia (including central China) (Choi et al. 2016). Increasing (decreasing) over-land translation distance of landfall TCs over China (excluding China) is likely to enlarge (lessen) the likelihood of TC-induced flooding, but simultaneously increase (decrease) the more beneficial drought-terminating impacts of TCs in inland areas of China (non-China parts of East Asia).

Code availability. All codes related to our results are available from the corresponding

author (Xihui Gu) on reasonable request.

Data availability. Tropical cyclone track data from the International Best Track Archive for Climate Stewardship and Hong Kong Observatory are available at https://doi.org/10.25921/82ty-9e16, from the China Meteorological Administration at http://tcdata.typhoon.org.cn, from Joint typhoon Warning Center at https://www.metoc.navy.mil/jtwc/jtwc.html?best-tracks, and from the Japan Meteorological Agency at http://www.jma.go.jp/jma/jma-eng/jma-center/rsmc-hp-pub-eg/besttrack.html. The ERA5 reanalysis data are available at https://www.ecmwf.int/en/forecasts/datasets/reanalysis-datasets/era5. Monthly climate indices (i.e. Nino 3.4 and PDO) are obtained from the Global Climate Observing System at https://psl.noaa.gov/gcos_wgsp/Timeseries/.

Acknowledgments

This study is supported by the Strategic Priority Research Program Grant of the Chinese Academy of Sciences (Grant No. XDA19070402), the National Key Research and Development Program of China (Grant Nos. 2019YFA0606900 and 2018YFA0605603), and the National Natural Science Foundation of China (Grant Nos. U1911205 and 41901041). X. Gu is supported by the China Scholarship Council.

Author contributions

X. Gu and Q. Zhang designed this study; L. Wang and X. Gu analyzed data and wrote the first draft of this paper; all authors contributed to the analysis, explaining the results and editing the final draft.

Additional information

Supplementary material for this article is also available.

Competing interests

The authors declare that they have no competing interests.

826

827 **References**

828 Aryal, Y. N., G. Villarini, W. Zhang, and G. A. Vecchi, 2018: Long term changes in
829 flooding and heavy rainfall associated with North Atlantic tropical cyclones:
830 Roles of the North Atlantic Oscillation and El Nino-Southern Oscillation. *J.*
831 *Hydrol.*, **559**, 698–710, https://doi.org/10.1016/j.jhydrol.2018.02.072.

832 Atkinson, G. D., and C. R. Holliday, 1977: Tropical Cyclone Minimum Sea Level
833 Pressure/Maximum Sustained Wind Relationship for the Western North Pacific.
834 *Mon. Weather Rev.*, **105**, 421–427, https://doi.org/10.1175/1520-
835 0493(1977)105<0421:TCMSLP>2.0.CO;2.

836 Bell, R., K. Hodges, P. L. Vidale, J. Strachan, and M. Roberts, 2014: Simulation of
837 the Global ENSO-Tropical Cyclone Teleconnection by a High-Resolution
838 Coupled General Circulation Model. *J. Clim.*, **27**, 6404–6422,
839 https://doi.org/10.1175/JCLI-D-13-00559.1.

840 Camargo, S. J., and A. H. Sobel, 2005: Western North Pacific tropical cyclone
841 intensity and ENSO. *J. Clim.*, **18**, 2996–3006,
842 https://doi.org/10.1175/JCLI3457.1.

843 Camargo, S. J., K. A. Emanuel, and A. H. Sobel, 2007a: Use of a Genesis Potential
844 Index to Diagnose ENSO Effects on Tropical Cyclone Genesis. *J. Clim.*, **20**,
845 4819–4834, https://doi.org/10.1175/JCLI4282.1.

846 Camargo, S. J., A. W. Robertson, S. J. Gaffney, P. Smyth, and M. Ghil, 2007b:
847 Cluster analysis of typhoon tracks. Part I: General properties. *J. Clim.*, **20**, 3635–
848 3653, https://doi.org/10.1175/JCLI4188.1.

849 CAMARGO, S. J., A. H. SOBEL, A. G. BARNSTON, and K. A. EMANUEL, 2007:
850 Tropical cyclone genesis potential index in climate models. *Tellus A*, **59**, 428–
851 443, https://doi.org/https://doi.org/10.1111/j.1600-0870.2007.00238.x.

852 CHAN, J. C. L., and W. M. GRAY, 1982: TROPICAL CYCLONE MOVEMENT
853 AND SURROUNDING FLOW RELATIONSHIPS. *Mon. Weather Rev.*, **110**,
854 1354–1374, https://doi.org/10.1175/1520-
855 0493(1982)110<1354:TCMASF>2.0.CO;2.

856 Chan, K. T. F., 2019: Are global tropical cyclones moving slower in a warming
857 climate? *Environ. Res. Lett.*, **14**, 104015, https://doi.org/10.1088/1748-
858 9326/ab4031.
859 Chand, S. S., K. J. Tory, H. Ye, and K. J. E. Walsh, 2017: Projected increase in El
860 Nino-driven tropical cyclone frequency in the Pacific. *Nat. Clim. Chang.*, **7**, 123-
861 +, https://doi.org/10.1038/NCLIMATE3181.
862 Chavas, D., and J. Chen, 2020: Hurricanes last longer on land in a warming world.
863 *Nature*, **587**, 200–201, https://doi.org/10.1038/d41586-020-03118-2.
864 Chen, J., and Coauthors, 2021: Changing Impacts of Tropical Cyclones on East and
865 Southeast Asian Inland Regions in the Past and a Globally Warmed Future
866 Climate. *Front. Earth Sci.*, **9**, https://doi.org/10.3389/feart.2021.769005.
867 Chen, X., and L. Wu, 2016: Topographic Influence on the Motion of Tropical
868 Cyclones Landfalling on the Coast of China. *Weather Forecast.*, **31**, 1615–1623,
869 https://doi.org/10.1175/WAF-D-16-0053.1.
870 ——, ——, and J. Zhang, 2011: Increasing duration of tropical cyclones over China.
871 *Geophys. Res. Lett.*, **38**, https://doi.org/https://doi.org/10.1029/2010GL046137.
872 Cheung, K. K. W., 2004: Large-scale environmental parameters associated with
873 tropical cyclone formations in the western North Pacific. *J. Clim.*, **17**, 466–484,
874 https://doi.org/10.1175/1520-0442(2004)017<0466:LEPAWT>2.0.CO;2.
875 Choi, J.-W., Y. Cha, and J.-Y. Kim, 2016: Reverse relationship between drought of
876 mid-latitudes in East Asia and Northwest Pacific tropical cyclone genesis
877 frequency in summer. *Geosci. Lett.*, **3**, 29, https://doi.org/10.1186/s40562-016-
878 0061-4.
879 Choy, C., M. Wu, and T. Lee, 2020: Assessment of the damages and direct economic
880 loss in Hong Kong due to Super Typhoon Mangkhut in 2018. *Trop. Cyclone Res.*
881 *Rev.*, **9**, 193–205, https://doi.org/https://doi.org/10.1016/j.tcrr.2020.11.001.
882 Corporal-Lodangco, I. L., L. M. Leslie, and P. J. Lamb, 2016: Impacts of ENSO on
883 Philippine Tropical Cyclone Activity. *J. Clim.*, **29**, 1877–1897,
884 https://doi.org/10.1175/JCLI-D-14-00723.1.
885 Czajkowski, J., G. Villarini, E. Michel-Kerjan, and J. A. Smith, 2013: Determining

tropical cyclone inland flooding loss on a large scale through a new flood peak ratio-based methodology. *Environ. Res. Lett.*, **8**, https://doi.org/10.1088/1748-9326/8/4/044056.

Elsner, J., 2003: Tracking Hurricanes. *Bull. Am. Meteorol. Soc. - BULL AMER METEOROL SOC*, **84**, 353–356, https://doi.org/10.1175/BAMS-84-3-353.

Emanuel, K., C. DesAutels, C. Holloway, and R. Korty, 2004: Environmental control of tropical cyclone intensity. *J. Atmos. Sci.*, **61**, 843–858, https://doi.org/10.1175/1520-0469(2004)061<0843:ECOTCI>2.0.CO;2.

——, R. Sundararajan, and J. Williams, 2008: Hurricanes and global warming - Results from downscaling IPCC AR4 simulations. *Bull. Am. Meteorol. Soc.*, **89**, 347-+, https://doi.org/10.1175/BAMS-89-3-347.

Emanuel, K. A., 1995: Sensitivity of tropical cyclones to surface exchange coefficients and a revised steady-state model incorporating eye dynamics. *J. Atmos. Sci.*, **52**, 3969–3976.

——, 2005: Increasing destructiveness of tropical cyclones over the past 30 years. *Nature*, **436**, 686–688.

——, 2007: Environmental factors affecting tropical cyclone power dissipation. *J. Clim.*, **20**, 5497–5509.

Enrico, S., G. Silvio, B. Alessio, P. Daniele, C. Annalisa, V. G. A., and N. Antonio, 2020: The typhoon-induced drying of the Maritime Continent. *Proc. Natl. Acad. Sci.*, **117**, 3983–3988, https://doi.org/10.1073/pnas.1915364117.

Frank, W. M., and E. A. Ritchie, 2001: Effects of vertical wind shear on the intensity and structure of numerically simulated hurricanes. *Mon. Weather Rev.*, **129**, 2249–2269, https://doi.org/10.1175/1520-0493(2001)129<2249:EOVWSO>2.0.CO;2.

Franklin, J. L., S. E. Feuer, J. Kaplan, and S. D. Aberson, 1996: Tropical cyclone motion and surrounding flow relationships: Searching for beta gyres in omega dropwindsonde datasets. *Mon. Weather Rev.*, **124**, 64–84, https://doi.org/10.1175/1520-0493(1996)124<0064:TCMASF>2.0.CO;2.

Gudmundsson, L., S. I. Seneviratne, and X. B. Zhang, 2017: Anthropogenic climate

change detected in European renewable freshwater resources. *Nat. Clim. Chang.*, **7**, 813-+, https://doi.org/10.1038/NCLIMATE3416.

Guo, Y. P., and Z. M. Tan, 2018: Westward migration of tropical cyclone rapid-intensification over the Northwestern Pacific during short duration El Nino. *Nat. Commun.*, **9**, https://doi.org/10.1038/s41467-018-03945-y.

Hamed, K. H., and A. R. Rao, 1998: A modified Mann-Kendall trend test for autocorrelated data. *J. Hydrol.*, **204**, 182–196, https://doi.org/10.1016/S0022-1694(97)00125-X.

He, H. Z., J. Yang, D. Y. Gong, R. Mao, Y. Q. Wang, and M. N. Gao, 2015: Decadal changes in tropical cyclone activity over the western North Pacific in the late 1990s. *Clim. Dyn.*, **45**, 3317–3329, https://doi.org/10.1007/s00382-015-2541-1.

Hiroyuki, M., D. T. L., C. W. F., Z. Ming, X. Baoqiang, and H. Pang-Chi, 2020: Detected climatic change in global distribution of tropical cyclones. *Proc. Natl. Acad. Sci.*, **117**, 10706–10714, https://doi.org/10.1073/pnas.1922500117.

Kam, J. H., J. Sheffield, X. Yuan, and E. F. Wood, 2013: The Influence of Atlantic Tropical Cyclones on Drought over the Eastern United States (1980-2007). *J. Clim.*, **26**, 3067–3086, https://doi.org/10.1175/JCLI-D-12-00244.1.

Knutson, T., and Coauthors, 2019: Tropical Cyclones and Climate Change Assessment: Part I: Detection and Attribution. *Bull. Am. Meteorol. Soc.*, **100**, 1987–2007, https://doi.org/10.1175/BAMS-D-18-0189.1.

——, and Coauthors, 2020: Tropical Cyclones and Climate Change Assessment: Part II: Projected Response to Anthropogenic Warming. *Bull. Am. Meteorol. Soc.*, **101**, E303–E322, https://doi.org/10.1175/BAMS-D-18-0194.1.

Knutson, T. R., and Coauthors, 2013: Dynamical Downscaling Projections of Twenty-First-Century Atlantic Hurricane Activity: CMIP3 and CMIP5 Model-Based Scenarios. *J. Clim.*, **26**, 6591–6617, https://doi.org/10.1175/JCLI-D-12-00539.1.

Kossin, J. P., 2018: A global slowdown of tropical-cyclone translation speed. *Nature*, **558**, 104-+, https://doi.org/10.1038/s41586-018-0158-3.

Kossin, J. P., K. A. Emanuel, and G. A. Vecchi, 2014: The poleward migration of the

location of tropical cyclone maximum intensity. *Nature*, **509**, 349–352, https://doi.org/10.1038/nature13278.

Lai, Y. C., and Coauthors, 2020: Greater flood risks in response to slowdown of tropical cyclones over the coast of China. *Proc. Natl. Acad. Sci. U. S. A.*, **117**, 14751–14755, https://doi.org/10.1073/pnas.1918987117.

Lanzante, J. R., 2019: Uncertainties in tropical-cyclone translation speed. *Nature*, **570**, E6–E15, https://doi.org/10.1038/s41586-019-1223-2.

Lee, M. H., C. H. Ho, and J. H. Kim, 2010: Influence of tropical cyclone landfalls on spatiotemporal variations in typhoon season rainfall over South China. *Adv. Atmos. Sci.*, **27**, 443–454, https://doi.org/10.1007/s00376-009-9106-3.

Lee, T., C. Y. Leung, M. Kok, and H. Chan, 2012: The Long Term Variations of Tropical Cyclone Activity in the South China Sea and the Vicinity of Hong Kong. *Trop. Cyclone Res. Rev.*, **1**, 277–292, https://doi.org/https://doi.org/10.6057/2012TCRR02.01.

Li, L., and P. Chakraborty, 2020: Slower decay of landfalling hurricanes in a warming world. *Nature*, **587**, 230-+, https://doi.org/10.1038/s41586-020-2867-7.

Liu, L., and Y. Wang, 2020: Trends in Landfalling Tropical Cyclone–Induced Precipitation over China. *J. Clim.*, **33**, 2223–2235, https://doi.org/10.1175/JCLI-D-19-0693.1.

Lu, X., H. Yu, M. Ying, B. Zhao, S. Zhang, L. Lin, L. Bai, and R. Wan, 2021: Western North Pacific tropical cyclone database created by the China Meteorological Administration. *Adv. Atmos. Sci.*, **38**, 690–699, https://doi.org/10.1007/s00376-020-0211-7.

Maxwell, J. T., J. T. Ortegren, P. A. Knapp, and P. T. Soulé, 2013: Tropical Cyclones and Drought Amelioration in the Gulf and Southeastern Coastal United States. *J. Clim.*, **26**, 8440–8452, https://doi.org/10.1175/JCLI-D-12-00824.1.

Moon, I.-J., S.-H. Kim, and J. C. L. Chan, 2019: Climate change and tropical cyclone trend. *Nature*, **570**, E3–E5, https://doi.org/10.1038/s41586-019-1222-3.

Nakamura, J., U. Lall, Y. Kushnir, and S. J. Camargo, 2009: Classifying North Atlantic Tropical Cyclone Tracks by Mass Moments. *J. Clim.*, **22**, 5481–5494,

https://doi.org/10.1175/2009JCLI2828.1.

Nayak, M. A., G. Villarini, and A. A. Bradley, 2016: Atmospheric Rivers and Rainfall during NASA's Iowa Flood Studies (IFloodS) Campaign. *J. Hydrometeorol.*, **17**, 257–271, https://doi.org/10.1175/JHM-D-14-0185.1.

Pettitt, A. N., 1979: A Non-Parametric Approach to the Change-Point Problem. *J. R. Stat. Soc. Ser. C (Applied Stat.*, **28**, 126–135, https://doi.org/10.2307/2346729.

Roderick, M. L., L. D. Rotstayn, G. D. Farquhar, and M. T. Hobbins, 2007: On the attribution of changing pan evaporation. *Geophys. Res. Lett.*, **34**, https://doi.org/10.1029/2007GL031166.

Schenkel, B. A., and R. E. Hart, 2015: An Examination of the Thermodynamic Impacts of Western North Pacific Tropical Cyclones on Their Tropical Tropospheric Environment. *J. Clim.*, **28**, 7529–7560, https://doi.org/10.1175/JCLI-D-14-00780.1.

Shen, Y., Y. Sun, Z. Zhong, K. Liu, and J. Shi, 2018: Sensitivity Experiments on the Poleward Shift of Tropical Cyclones over the Western North Pacific under Warming Ocean Conditions. *J. Meteorol. Res.*, **32**, 560–570, https://doi.org/10.1007/s13351-018-8047-0.

Simpson, R. H., and H. Riehl, 1981: *The Hurricane and Its Impact*. 398 pp.

Sriver, R. L., and M. Huber, 2007: Observational evidence for an ocean heat pump induced by tropical cyclones. *Nature*, **447**, 577–580, https://doi.org/10.1038/nature05785.

Studholme, J., A. V Fedorov, S. K. Gulev, K. Emanuel, and K. Hodges, 2022: Poleward expansion of tropical cyclone latitudes in warming climates. *Nat. Geosci.*, **15**, 14–28, https://doi.org/10.1038/s41561-021-00859-1.

Sun, X., R. J. Greatbatch, W. Park, and M. Latif, 2010: Two major modes of variability of the East Asian summer monsoon. *Q. J. R. Meteorol. Soc.*, **136**, 829–841, https://doi.org/https://doi.org/10.1002/qj.635.

Villarini, G., R. Goska, J. A. Smith, and G. A. Vecchi, 2014: North Atlantic tropical cyclone and U.S. flooding. *Bull. Am. Meteorol. Soc.*, **95**, 1381–1388, https://doi.org/10.1175/BAMS-D-13-00060.1.

Vincent, E. M., M. Lengaigne, G. Madec, J. Vialard, G. Samson, N. C. Jourdain, C. E. Menkes, and S. Jullien, 2012: Processes setting the characteristics of sea surface cooling induced by tropical cyclones. *J. Geophys. Res. Ocean.*, **117**, https://doi.org/https://doi.org/10.1029/2011JC007396.

Walsh, K., K. Nguyen, and J. McGregor, 2005: Climate change, tropical cyclones and ENSO. *85th AMS Annu. Meet. Am. Meteorol. Soc. - Comb. Prepr.*, **86**.

Wang, S., and R. Toumi, 2021: Recent migration of tropical cyclones toward coasts. *Science (80-.).*, **371**, 514-+, https://doi.org/10.1126/science.abb9038.

Wang, X. D., and H. L. Liu, 2016: PDO modulation of ENSO effect on tropical cyclone rapid intensification in the western North Pacific. *Clim. Dyn.*, **46**, 15–28, https://doi.org/10.1007/s00382-015-2563-8.

——, C. Z. Wang, L. P. Zhang, and X. Wang, 2015: Multidecadal Variability of Tropical Cyclone Rapid Intensification in the Western North Pacific. *J. Clim.*, **28**, 3806–3820, https://doi.org/10.1175/JCLI-D-14-00400.1.

Wang, Y., and C. C. Wu, 2004: Current understanding of tropical cyclone structure and intensity changes - a review. *Meteorol. Atmos. Phys.*, **87**, 257–278, https://doi.org/10.1007/s00703-003-0055-6.

Yamaguchi, M., J. C. L. Chan, I. J. Moon, K. Yoshida, and R. Mizuta, 2020: Global warming changes tropical cyclone translation speed. *Nat. Commun.*, **11**, https://doi.org/10.1038/s41467-019-13902-y.

Yang, L., M. F. Liu, J. A. Smith, and F. Q. Tian, 2017: Typhoon Nina and the August 1975 Flood over Central China. *J. Hydrometeorol.*, **18**, 451–472, https://doi.org/10.1175/JHM-D-16-0152.1.

——, S. Chen, C. Z. Wang, D. X. Wang, and X. Wang, 2018: Potential impact of the Pacific Decadal Oscillation and sea surface temperature in the tropical Indian Ocean-Western Pacific on the variability of typhoon landfall on the China coast. *Clim. Dyn.*, **51**, 2695–2705, https://doi.org/10.1007/s00382-017-4037-7.

Zehr, R. M., 2003: Environmental vertical wind shear with Hurricane Bertha (1996). *Weather Forecast.*, **18**, 345–356, https://doi.org/10.1175/1520-0434(2003)018<0345:EVWSWH>2.0.CO;2.

Zhang, G., H. Murakami, T. R. Knutson, R. Mizuta, and K. Yoshida, 2020: Tropical cyclone motion in a changing climate. *Sci. Adv.*, **6**, https://doi.org/10.1126/sciadv.aaz7610.

Zhang, Q., X. H. Gu, J. F. Li, P. J. Shi, and V. P. Singh, 2018: The Impact of Tropical Cyclones on Extreme Precipitation over Coastal and Inland Areas of China and Its Association to ENSO. *J. Clim.*, **31**, 1865–1880, https://doi.org/10.1175/JCLI-D-17-0474.1.

Zhang, Q. A., L. G. Wu, and Q. F. Liu, 2009: TROPICAL CYCLONE DAMAGES IN CHINA 1983-2006. *Bull. Am. Meteorol. Soc.*, **90**, 489-+, https://doi.org/10.1175/2008BAMS2631.1.

Zhu, Y.-J., and J. M. Collins, 2021: Recent Rebounding of the Post-Landfall Hurricane Wind Decay Period Over the Continental United States. *Geophys. Res. Lett.*, **48**, e2020GL092072, https://doi.org/https://doi.org/10.1029/2020GL092072.

2013: Drought-busting cyclones. *Nature*, **499**, 128, https://doi.org/10.1038/499128c.